ACS APPLIED MATERIALS & INTERFACES

Research Article

www.acsami.org

Reactive Molecular Dynamics Study of Chloride Ion Interaction with Copper Oxide Surfaces in Aqueous Media

Byoungseon Jeon,*[,†] Subramanian K. R. S. Sankaranarayanan,[‡] Adri C. T. van Duin,[§] and Shriram Ramanathan[†]

[†]School of Engineering and Applied Sciences, Harvard University, Cambridge, Massachusetts 02138, United States

[‡]Center for Nanoscale Materials, Argonne National Laboratory, Argonne, Illinois 60439, United States

[§]Department of Mechanical and Nuclear Engineering, Pennsylvania State University, Pennsylvania 16802, United States

ABSTRACT: Using reactive force-field (ReaxFF) and molecular dynamics simulation, we study atomistic scale chloride ion adsorption and transport through copper oxide thin films under aqueous conditions. The surface condition of passive oxide film plays a key role in chloride ion adsorption and facilitates initial adsorption when surface corrosion resistance is low. Using implemented surface defects, the structural evolution of the copper oxide film from thinning to breakdown is investigated. In addition to chemical thinning of passive film, extended defects in the metal substrate are observed, at high concentration of adsorbed chloride ions. The initial stage of breakdown is associated with rapid depletion of adjacent chloride ions, which creates a locally deficient environment of chloride ions in the solution. The dissolved copper cations gain higher charge upon interaction with chloride ions. Owing to the increased Coulomb interactions resulted from dissolved copper ions and locally low density of chloride ions, far-field chloride ions would diffuse into the local corrosion sites, thereby promoting further corrosion.

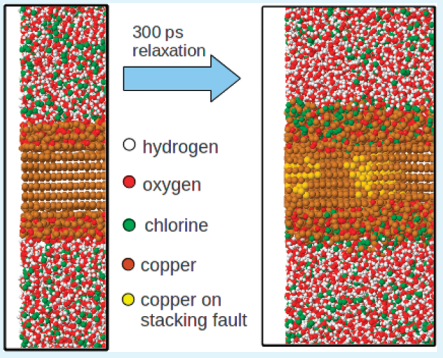

KEYWORDS: *ReaxFF, reactive molecular dynamics, aqueous corrosion, copper oxide, pitting, chloride*

INTRODUCTION

The chemical reactions that occur at the metal oxide−aqueous solution interfaces have been a subject of immense scientific interest because of their importance in a variety of fields, including catalysis, surface chemistry, metal-oxide crystal growth to name a few.[1−6] The chemical interactions occurring at the interface of metal-oxide and aqueous media are complex and fundamental atomic scale understanding of these phenomena is a contemporary problem.[1−5] Specifically, there are a number of fundamental questions, which are worth considering, such as: the effect of water and solute ions on the structure, composition, and reactivity of surface sites including defects, the local speciation of metal ions and anions in the solution, the charge transfer dynamics at the metal oxide−water interface, the mechanisms of ion adsorption and transport, and their effect on surface atomic and electronic structure.

Using a model system consisting of copper oxide thin film on copper interacting with chloride ions in aqueous media, we attempt to understand representative processes that occur at the interface of passive copper oxide and aqueous media. These include processes such as initial adsorption and transport of aggressive anions through the oxide film, which play an important role in determining the stability and durability of the underlying material.

Copper remains one of the most important industrial metals because of its high electrical and thermal conductivities, mechanical workability and its relatively noble properties. Metallic copper is generally covered with a surface oxide under normal ambient, and has been studied extensively, because of its importance in electronics, catalysis, and energy storage.[7−11] In electronics and communications, it is commonly employed as an interconnect. Additionally, it is used as piping component in domestic and industrial water utilities. Therefore, aqueous corrosion of copper and its inhibition in a wide variety of media, particularly when they contain chloride ions, is an important problem.

Under various aqueous environments, copper oxide film can interact with aggressive elements, such as halide ions, which can change their properties leading to loss of material strength and durability.[12,13] In particular, aqueous conditions are commonly encountered, and the corresponding electrochemical interactions must hence be understood.

Previous experimental and theoretical work has focused on understanding the interactions between Cu/CuO and Cl for two main reasons[14−22] First, it is well-known that chloride ions are aggressive to copper and its alloys. The interaction of Cu with the chloride ions leads to the formation of an unstable film of CuCl and other water-soluble chloride complexes, $CuCl_2$, $CuCl_3$.[23] It has been reported that even trace amounts of Cl^- ions can cause corrosion and degradation of copper. Second,

Received: September 30, 2011
Accepted: February 28, 2012
Published: February 28, 2012

   dx.doi.org/10.1021/am201345v | *ACS Appl. Mater. Interfaces* 2012, 4, 1225−1232

copper and its alloys are used in applications such as piping and delivery of water for domestic and industrial purposes. They are thus exposed to medium where Cl^- ions are present.[24] Despite the relatively noble potential of copper, its corrosion is known to take place at a significant rate in seawater and aqueous environments containing chloride ions.[25−29] Available studies indicate that at chloride concentrations lower than 1 M, the dissolution of copper occurs through formation of CuCl, which is not protective enough and is therefore converted to the soluble $CuCl_2^-$ by reacting with excess chloride.[30] On the other hand, at concentrations higher than 1 M, higher cuprous complexes such as $CuCl_3$ and $CuCl_4$ are formed, in addition to chlorides, such as CuCl and $CuCl_2$.[31] Although it is generally accepted that anodic dissolution of copper in chloride environments is influenced by the chloride ions' concentration, the atomic scale mechanism of corrosion initiation is not well understood. Specifically, the exact charge transfer mechanism, details of ion adsorption and transport mechanism as well as the sequence of steps that lead to initiation and propagation of corrosion at the atomistic length scales remain unclear.

Atomistic molecular dynamics simulations and first-principles studies have been used in the past to understand the dynamics and energetics of chloride ion adsorption onto the surface of passive oxides. These studies have explored the effect of chloride ion concentration, ambient temperature, and components of aqueous media but interactions between copper oxides and aggressive aqueous media has not been studied yet, because of the complexity in atomistic scale modeling.[32−34] As discussed by Stampfl et al.,[35] since early stages of such aqueous interactions are determined in pico-second and nanometer scales, the corresponding atomistic scale analysis is essential to figure out subsequent behavior and characteristics. In particular, degradation mechanism of protective oxide layer on top of metal substrates is of great importance, to understand the basic characteristics of aqueous corrosion. Further failure of oxide results in pitting, which leads to structural stability. In a recent study,[36] we have investigated direct interactions between pristine copper substrates and aqueous media, including the effect of chloride ions by reactive molecular dynamics (MD) simulations.

Here, we focus on the interaction between copper oxides and chloride ions in aqueous media and the role of oxide surface defects in the adsorption and subsequent kinetic phenomena. In many atomistic scale simulations, classical molecular dynamics has been favored due to capability in handling a large number of particles ($>1 \times 10^5$) but it is not suitable to handle chemical reactions of the current study due to fixed charge implementation. Metal cations and anions in aqueous media interact through charge transfer, producing chemical bonding or debonding, which is not implemented in most of classical MD approach. Quantum molecular dynamics might be an alternative but computational cost is high. To overcome those difficulties, reactive methods have been developed and employed in many chemical reaction problems. In the frame of classical molecular dynamics, variable charge or charge transfer scheme is implemented, and temporal evolution of charge states is accomplished. Among the various reactive methods, reactive force-field (ReaxFF)[37] implements features of quantum chemistry calculations, including molecular association/dissociation and charge transfer between cations and anions, and description of aqueous interaction of oxide surfaces with chloride ions is therefore made possible, including proton transfer[38,39] or proton swapping of water molecules. Detailed description of the employed method is discussed below.

In this study, we use potential parameters developed by van Duin et al.,[40,41] who have tested models of Cu−Cl interacting with water molecules and fitted the potential parameters to reproduce DFT/experimental results. Using ReaxFF, we have investigated temporal evolution of copper oxides and substrates in aqueous media, leading to the early stages of chemical failure of a copper oxide structure. To the best of our knowledge, this work represents the first atomistic scale simulations of aqueous corrosion of copper oxides with large statistics ($\sim 1 \times 10^5$), shedding light on understanding aqueous breakdown of copper oxides.

METHODS

We have implemented a parallel version of ReaxFF code using FORTRAN95 programming language. ReaxFF is a bond-order based empirical force field methods, which can be used to simulate bond breaking and formation during molecular dynamics simulations. ReaxFF combines this bond order/bond distance concept[42−44] with a polarizable, geometry-dependent charge calculation method.[45] Originally derived for hydrocarbons[37] ReaxFF has been developed for a wide range of materials, including the copper oxides and chlorides described in this manuscript.[40,41] Briefly, characteristics of quantum chemistry effect are employed in multiple-components of particle interactions as shown in eq 1, such as bond energy, over/under coordination, lone-pair energy, valence angle, torsion, hydrogen bond, van der Waals, and Coulomb.

$$E_{\text{total}} = E_{\text{bond}} + E_{\text{over}} + E_{\text{under}} + E_{\text{lp}} + E_{\text{val}} + E_{\text{tors}} + E_{\text{H}} + E_{\text{vdw}} + E_{\text{Coul}} \quad (1)$$

Temporal charges of cations/anions are also implemented using electronegativity equalization method[45,46] as shown in eq 2.

$$E(q) = \sum_i \left[\chi_i q_i + \eta_i q_i^2 + Tap(r_{ij}) k_c \frac{q_i q_j}{(r_{ij}^3 + \gamma_{ij}^{-3})^{1/3}} \right] \quad (2)$$

In the above equations, q, χ, η, $Tap(r)$, γ, and k_c are ion charge, electronegativity, atomic hardness, seventh-order taper function, shielding parameter, and dielectric constant, respectively. For a detailed description of the implementation we refer the reader to the work by Chenoweth et al.[47]

Most of the calculations have been done on Carbon clusters at Argonne National laboratory, which are equipped with dual Xeon E5540 processors (= eight cores) per node and infiniband 4X DDR interconnection. Intel Fortran compiler (12.0.2) with open-mpi library (1.4.2) has been employed. Coarse-grain parallelism has been applied using domain-decomposition method, splitting the unit cell into each computing node. Multiple-threading has been implemented using OpenMP,[48] as fine-grain parallelism. Once a piece of unit cell is assigned in each computing node, loops are forked along available processors and computation is accelerated. Detailed implementation of multiple-threading on molecular dynamics can be found from the work by Tarmyshov and Müller-Plathe.[49] Temperature control has been done with Berendsen thermostat.[50]

EFFECT OF OXIDE SURFACE CONDITION ON BREAKDOWN

We use copper substrates as a base metal, and Cu_2O is the surface oxide under consideration. Oxygen in the oxide competes with nearby halide elements, passivating and protecting the inner metal substrate. As discussed by Baroux,[51] a corrosion resistance varies depending on the surface condition of passive films. As shown in Figure 1, even for similar stoichiometry, corrosion resistance may change drastically depending on the surface interacting with aqueous media. Therefore, it is straightforward that lower surface corrosion resistance results when a local site has fewer surface oxygen atoms, facilitating chloride ion adsorption. Once chloride ions adsorb onto the passive film, it begins to bond with nearby copper cations by breaking existing copper−oxygen bonds, which leads to thinning of the passive film. To confirm the effect of surface condition, we have done the following tests.

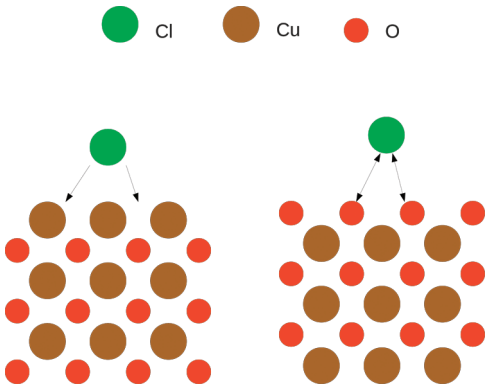

Figure 1. Effect of surface condition of oxide on initial adsorption by a chloride ion. If chloride ions interacts with bare copper (left, O-deficient surface), then adsorption is facilitated. If surface oxygen density is high (right, O-enriched surface), those oxygen atoms compete with chloride ions and protect the oxide film.

As shown in the left of Figure 2, 1008 copper atoms are configured with (111) orientation along surface normal, which is the base metal substrate. The metal is depicted as separate plates but they are connected by periodic boundary conditions (PBC). Then two 6−7 Å Cu_2O oxide thin films, each of which is composed of 768 Cu and 384 O atoms, are configured on each side of the substrate while the center of the unit-cell (between oxide films) will be filled with aqueous media. The two oxide films have the same stoichiometry but their surface orientations with respect to aqueous media are configured differently: the upper film (referred to as O-deficient surface) has a higher surface density of copper, whereas the lower film (O-enriched surface) has a higher surface density of O, by turning over the produced oxide lattice. As discussed in Figure 1, O-deficient/enriched surfaces will have different corrosion resistances. Note that the Cu_2O oxide models has been configured as asymmetric which could have generated a dipole moment. ReaxFF has variable charge implementation using EEM as shown above, such a dipole moment has been included in the computational modeling. However, periodic boundary conditions are configured and the copper substrate is fixed by neighboring (x/y direction) images. Therefore, tested copper oxides and substrates are not affected by the produced dipole moment.

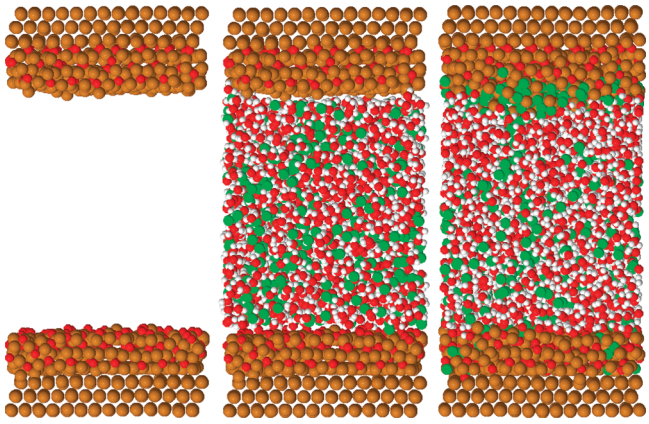

Figure 2. Configuration based on the oxide surface conditions. Left figure is the thermally relaxed structure of copper substrate and oxide thin film. The empty space is filled with 20 M Cl^- aqueous media as shown in center figure and relaxed at 300 K. Right figure shows 250 ps relaxation states and higher chloride ion adsorption onto upper oxide thin film, which has higher surface copper density (O-deficient surface). Lower oxide has higher surface O density (O-enriched surface), and chloride ion adsorption is resisted.

As an initial thermal perturbation, the metal substrate and oxide films had been relaxed in a 30.63 × 30.95 × 65 $Å^3$ unit cell for 10 ps at 300 K prior to filling the empty space with aqueous media. After thermal relaxation of base metal substrate and oxide thin films, the inner void space of the unit-cell has been filled with 1,269 H_2O and 228/457 chloride ions, equivalent to 10 and 20 M concentration, respectively, as shown in the middle of Figure 2. Overall, each simulation employs 6195/6424 particles for 10/20 M, respectively. Also, the employed aqueous media have been configured as neutral (pH 7), without any extra protons or hydroxyl molecules.

Molecular dynamics has inherent problems with respect to the time scales that can be achieved, due to the limit imposed by time steps (0.5 fs in this work). Most of the corrosion issues may appear at low chloride concentrations and their time range is likely to be more than several seconds, which is not accessible to atomistic modeling yet. In other words, available statistics is limited in atomistic scale simulations and low concentrations like 5 M may not yield any significant result in the simulated time scale (300 ps). Higher concentrations of 10 and 20 M have been thus used so that we could observe the passive oxide breakdown within the time scales that are accessible to the MD simulations. Therefore, even though the available concentration limit of chloride ions at room temperature is reported to be ∼10 M,[52] a locally extreme condition as 20 M is assumed to accelerate corrosion kinetics owing to the several orders of magnitude difference between the MD time-scale and the actual corrosion processes.[35]

Using a canonical ensemble at 300 K, the configured structures for investigating aqueous corrosion have been relaxed for 250 ps. The relaxed structure is shown on the right-hand side of Figure 2. Chloride ion adsorption is facilitated on the O-deficient surface, which is the oxide structure having low surface density of oxygen. As a result, the O-deficient surface shows much more adsorbed chloride ions compared to the O-enriched surface, showing distinct thinning of oxide film.

Figure 3 shows the adsorbed chloride ions and copper oxide/substrates, without aqueous media, to aid visualization. As discussed above, the O-deficient surface has much more adsorbed chloride ions than the O-enriched surface, at both

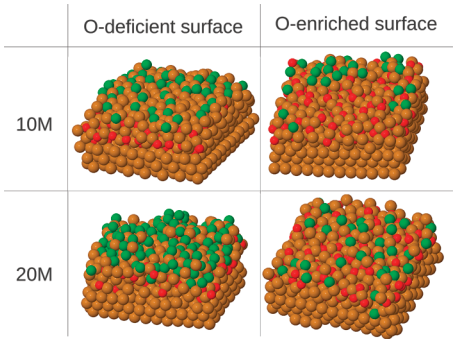

Figure 3. Adsorbed chloride ions on the oxide thin film at 250 ps relaxation with 10 M (top)/20 M (bottom) Cl^- concentration. Left figures are O-deficient surfaces, whereas right figures are O-enriched surfaces, which show distinct differences because of surface conditions and chloride ion concentration.

10 and 20 M concentrations. As chloride ion concentration is higher at 20 M, more adsorbed chloride ions are observed in both the exposed oxide surfaces, compared to 10 M concentration results. Looking at the evolution of oxide thinning, a chloride ion enables removal of copper from copper-oxide as it adsorbs on top of the oxide layer. Corresponding copper atoms are dissolved and brought off from the plane of oxide film. Our results appear consistent with pitting corrosion mechanism suggested by El Warraky et al.,[29] who reported that dissolving copper ions pass through $CuCl_2^-$ soluble complex, by using potentiostatic polarization and X-ray photoelectron spectroscopy. A closer analysis of the morphology of adsorbed chloride ions suggests that chloride ion adsorption sites seem to facilitate further adsorption, yielding nonuniform Cu−Cl complexes, which subsequently dissolve in the aqueous media. Compared to oxygen passivation,[53] we find that the lateral diffusion or homogenization of Cu−Cl layer is not significant. After dissolution from copper oxides, copper ions attain higher charge because of the strong electronegativity of chloride ions, and subsequently may attract nearby chloride ions by Coulomb interactions, elevating nonuniform chloride ion adsorption.

To estimate the magnitude of chloride ion adsorption, we calculated average charges of copper, as shown in Figure 4, on O-deficient/enriched surfaces, which are shown in Figure 3. Looking at the results of 10 M condition, the O-deficient surface shows higher charge states from the beginning, by promoting initial chloride ion interactions. The difference between O-deficient/enriched surface charge states is quite

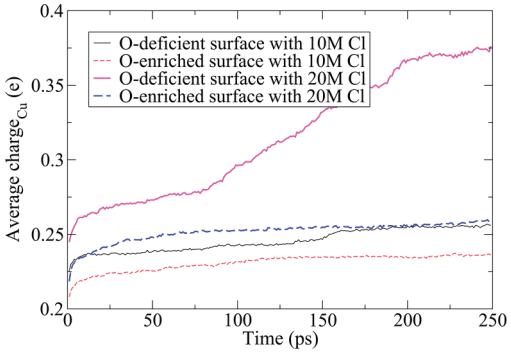

Figure 4. Evolution of average charge of copper atoms at O-deficient/enriched surfaces, including copper atoms from oxide and substrate.

consistent, indicating that corrosion or passivity breakdown is not so significant. Similar behavior is found in 20 M simulations, as the O-deficient surface is favored for initial chloride adsorption but the temporal evolution shows differences. Charge state of the O-enriched surface is saturated after 50 ps, with a slight jump from the initial state. However, the O-deficient surface shows consistent increase with higher rate after 100 ps. For further investigation of chloride adsorption on Cu surfaces, pair distribution functions of Cu−Cl and density distributions of Cu atoms are shown in left-hand side of Figure 5. Even though charge states of copper atoms at O-deficient

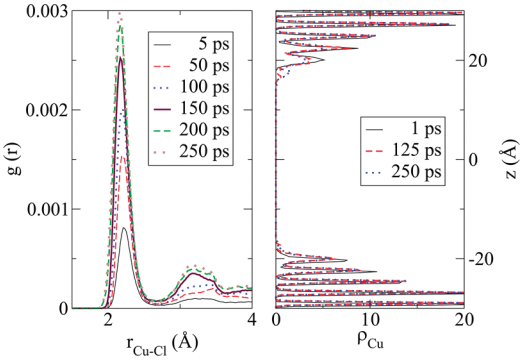

Figure 5. (Left) Pair distribution functions of Cu−Cl and (right) density distribution of copper atoms (unit: amu/Å^3) of 20 M Cl^- concentration simulations.

surface keep increasing, Cu−Cl interactions become saturated. This implies that chlorination of copper is increasing, from CuCl to $CuCl_2$ or $CuCl_3$. Also the increase of charge of copper atoms has been confirmed by inspection of each particle. Higher charge states of copper will attract far-field anions by higher Coulomb interactions, facilitating further corrosion.

In addition to the charge evolution, distributions of copper atoms have been studied in order to observe chemical thinning of oxide films. Density distribution of copper is shown in right-hand side of Figure 5 and compared to the initial state. We clearly observe smeared distributions of copper atoms at 250 ps relaxation around [18:20] of z-positions. Coupled with increasing charge states, those results show how the early stages of chemical thinning evolve along temporal trajectories.

Even though initial adsorption of chloride ions and chemical thinning of oxide is observed from the simulations above, the complete breakdown of passive film is not observed in the above simulations and more realistic configuration of simulations is required to study the structural evolution of oxide film during its interaction with chloride ions in aqueous media. The simulations discussed in the subsequent section discuss the implementation of surface defects to facilitate chloride ion adsorption.

LARGE-SCALE SIMULATIONS OF OXIDE STRUCTURAL EVOLUTION

From the initial simulations above, we can clearly see the importance of surface condition and thinning of oxide thin film. To observe the structural evolution of the passive oxide thin film until its complete breakdown, we configure larger aqueous simulation sets and introduce defective surface sites. Because of surface reconstruction or thermal effect, it is possible that a fraction of the surface sites in the oxide thin film may turn defective thereby favoring chloride ion adsorption and thus

have lower corrosion resistance,. Assuming such reconstruction, we can produce a local site that has surface defects in the form of bare copper atoms on top of the oxide, as shown in Figure 6.

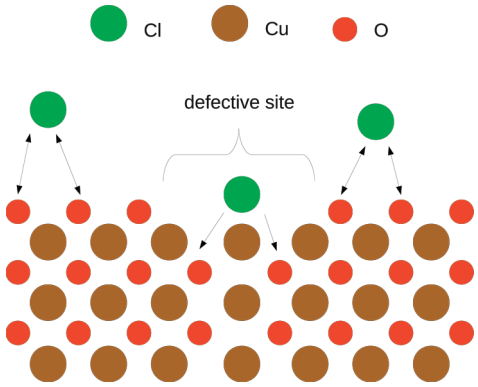

Figure 6. Different chloride ion interactions based on surface conditions of oxide film. If the surface density of copper is locally higher than elsewhere, the site (center) attracts nearby chloride ions easier than other sites (left and right), whereas chloride ions will compete with surface oxygen atoms when density of surface oxygen is high (left and right).

As in the above test, a copper substrate and passive oxide films on top and bottom have been configured using 12 960 copper atoms and 2640 O atoms on a 81.68 × 88.43 × 90 $Å^3$ unit cell. They have been first thermally relaxed at 300 K for 10 ps. Then top oxygen atoms on oxide have been removed from the edge with radius of 8 Å, to yield a circular surface defect as shown in the left of Figure 7. A unit cell has periodic boundary

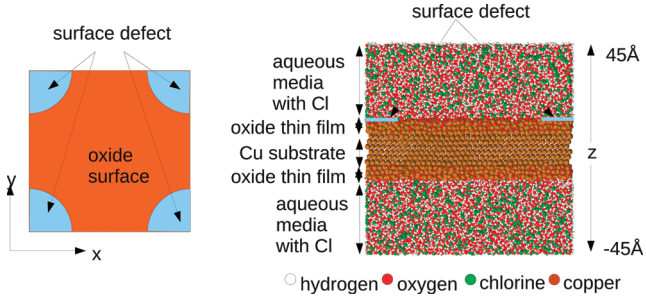

Figure 7. Implementation of surface defect (sites of higher copper surface density) on oxide thin film. Left figure shows how a circular defect is configured on surface oxide thin film with periodic boundary condition. Right figure shows the initial side-view of the unit cell.

conditions and those surface defects are connected as a single circular defective site. Then void space has been filled with 15 708 H_2O and 2827/5655 Cl^-, equivalent to 10/20 M concentration, respectively. Summarizing, a unit cell is filled with 65 525/68 353 particles for 10/20 M Cl^- concentration conditions. Initial configuration of the unit cell is shown in the right of Figure 7. Each concentration set has been relaxed for 300 ps with 373 K, assuming boiling temperature to accelerate corrosion behavior in the time frame of MD. For high-performance computing, multiple-threading parallelization is coupled with standard domain decomposition method, using 16−32 CPUs.[54]

From the results of 10/20 M simulations, we observe that initial chloride ion adsorption is favored on the defective site, which has less corrosion resistance. 20 M concentration simulation results are shown in Figure 8, and it shows passive oxide thinning due to high chloride ion concentration. Not only

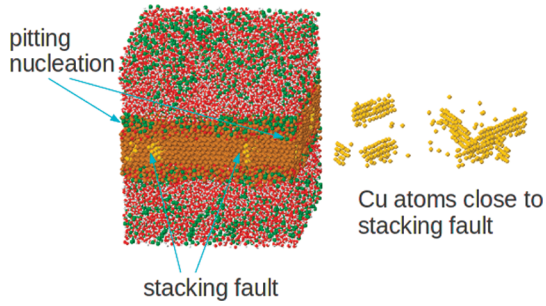

Figure 8. 300 ps relaxation of simulation with 20 M Cl-. Due to high chloride ion concentration, large fraction of surface shows chloride ion adsorption but still the implemented defective site has the highest chloride ion amount, yielding pitting nucleation. Also, higher chloride ion adsorption rate on localized site brings forth high stress and leads to defects in bulk substrate, around the defective site. Cu atoms close to the defects are marked yellow and redrawn in the right side for better visualization.

the defective sites but most of the oxide layers are also invaded by chloride ions. We find pitting nucleation below the defective site which shows that chloride ions reach the bulk substrate. In particular, not only the chemical thinning of passive layer and pitting nucleation, stacking fault of the bulk substrate is also observed, as shown in Figure 8. Calculating the number of opposing nearest pair particles,[55] Cu atoms which are close to stacking faults are determined and depicted in yellow. This is in accordance with experiments and finite element computations performed by Pidaparti et al.[56] who predicted enhanced stresses around a single pit/defect. Their study suggests that the stress distribution follow the pit/defect profile with maximum stresses being at the maximum pit/defect depth. The thin metal substrate combined with the high amount of adsorbed chloride ions result in high pressure being produced from the developing Cu−Cl clusters. The mechanical failure of passive oxide thin film is observed around the defective site. We can expect similar mechanical failure even for thicker substrates, such as delamination of oxide films and substrates, which is produced by bending stiffness mismatch of oxide layer and bulk substrates.

From the results of 10 M simulation, it is found that chloride ions at the defective site do not reach the interface between oxide and bulk substrate within the simulated time frame, because of lower chloride ion concentration. But we can expect that they will reach and nucleate pits if simulations are performed over longer time scales.

The evolution of average charge of copper species is shown in Figure 9. Even though the surface defect is introduced on the top side of the structure, the initial charge difference between top/bottom sides is minimal because the fraction of surface defect is not significant. As passive film is attacked by nearby chloride ions, the average charge on both sides increases monotonically. Unlike the initial state, charge difference across two sides increases accordingly, showing that top side, which has the surface defect, is charged higher than bottom side, at both 10 and 20 M conditions. In our preliminary study, the defective sites were present across the entire surface of oxides while they are a small fraction in the large-scale model. Therefore, effect of surface defect is minimal in the beginning

dx.doi.org/10.1021/am201345v | ACS Appl. Mater. Interfaces 2012, 4, 1225−1232

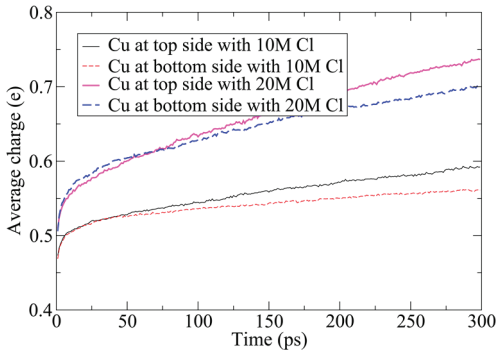

Figure 9. Average charge evolution of charged copper atoms at top/bottom side in 10/20 M Cl^- large-scale simulation sets.

but it promotes higher charge transfer or corrosion at longer simulation times.

The corrosion distribution in the top oxide layer is analyzed using the charge distribution of copper atoms, as shown in Figure 10. Projecting onto the x-y surface, charge distribution is

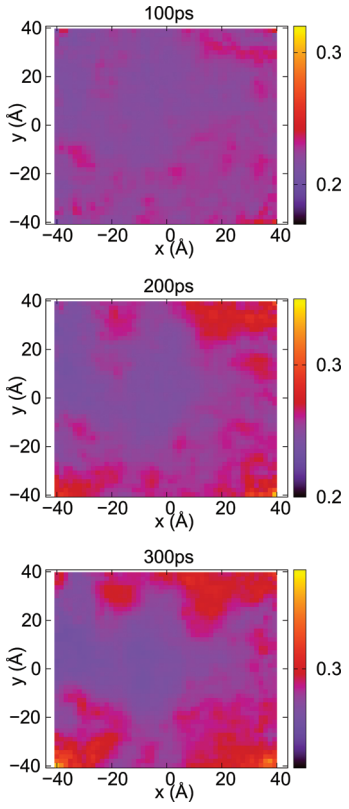

Figure 10. Charge distribution and evolution of top side copper atoms in 20 M Cl^- large-scale simulations sets at 100, 200, 300 ps relaxation. 50 × 50 grids are employed for projection.

shown at 100, 200, and 300 ps relaxation. As expected, highly charged copper atoms are found around the edges, which have defective sites. The center of surface shows relatively low charge states, implying less corrosion. We can confirm that if any local site initiates the corrosion or chloride ion adsorption, further corrosion is produced around that site. This reflects the finding by Leiva-García et al.,[57] who found that corrosion products catalyze the corrosion process.

Figure 11 shows the density distribution of copper and chloride at 1 and 300 ps, providing insights into the extent of

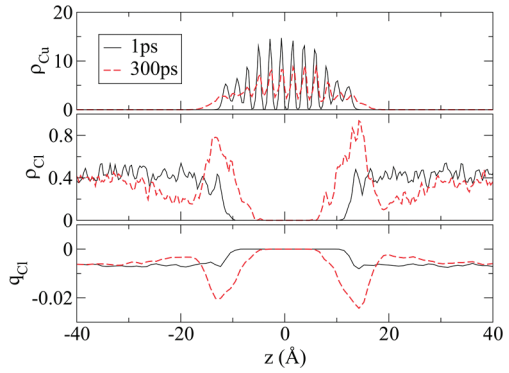

Figure 11. Density (ρ, amu/Å^3) distribution of copper atoms and chloride ions at 1 and 300 ps relaxation of 20 M Cl^- large-scale simulation. Charge (q, e/Å^3) distribution of chloride ions is shown at bottom.

corrosion upon starting with a clean surface. As copper atoms dissolve from the degraded passive film or bulk substrate, the density of copper is smeared at the top/bottom side of the structure. Chloride ions infiltrates into the oxide film and bulk substrate, yielding Cu−Cl clusters. Additionally, as brought out earlier, these Cu−Cl clusters further interact with additional chloride ions to form water-soluble $CuCl_2$ complexes. The chloride ion density profile therefore shows high density in the vicinity of passive film ([−13:−8],[8:13]). One significant result of chloride ion distribution is, that there are locally chloride-depleted regions in the aqueous media of the range [−25:−17] and [19:28]. As corrosion begins, it consumes neighboring chloride ions, and local density of chloride ions decreases. This can be confirmed from the charge distribution, which is shown in the bottom of Figure 11. Because of locally lowered density of chloride ions, we can expect chloride ions from far-field will diffuse into those depleted regions, resulting in further corrosion at the local site. However, such observation is beyond the time frame of MD and has not been simulated in this study.

We visually observed that Cu−Cl complexes are formed as aqueous corrosion evolves. Using pair distribution functions shown in the left of Figure 12, the formation of corrosion product Cu−Cl is confirmed to steadily increase with time. Also, this result reflects how protective surface oxide layers are

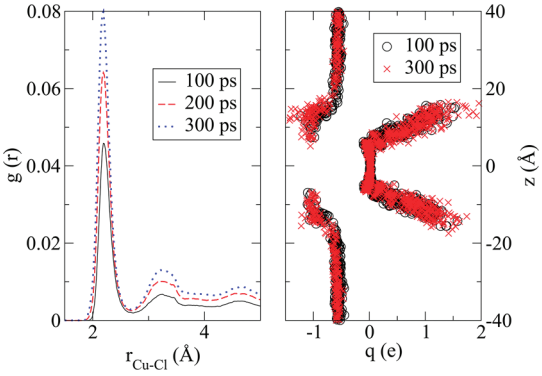

Figure 12. (Left) Pair distribution functions of Cu−Cl interactions at 100, 200, and 300 ps relaxation of 20 M Cl^- large-scale simulations. 2000 time steps are sampled. (Right) Cl^- ($q < 0$) and Cu^+ ($q > 0$) ion charge plots at 100 and 300 ps of 20 M Cl^- simulations. 10% of actual particles are plotted for better visualization.

dx.doi.org/10.1021/am201345v | ACS Appl. Mater. Interfaces 2012, 4, 1225−1232

disintegrated, as discussed above. Finally, snapshots of Cl^- and Cu^+ ion charge states are shown in the right of Figure 12. When chloride ions interact with copper cations, their charge states increase higher than when they are present in aqueous media. Also Cu cation charge increases as they interact with chloride ions. Therefore, in addition to the locally chloride deficient regions, highly charged copper cations will attract far-field chloride ions because of increased Coulomb interactions, thereby producing further corrosion.

CONCLUSIONS

To understand the chemical interaction at the interface between metal-oxide and aqueous media containing chloride ions, reactive molecular dynamics has been employed, allowing charge transfer between cations and anions, proton transfer between water molecules, breakdown of passive oxide films, and the formation of Cu−Cl complexes.

In the initial part of this study, different surface conditions of passive oxides have been tested and characteristics of chloride ion adsorption onto such surfaces have been studied. Local density of surface oxygen on copper oxide thin films determines its stability and corrosion resistance, yielding drastic change upon initial chloride adsorption. The atomistic simulations confirm the chemical thinning of oxide films under aggressive aqueous conditions, revealing the role of surface defects on passivity degradation. Nonuniform build-up of Cu−Cl complexes has been observed because of their low mobility.

Larger-scale substrates and oxide films are then configured with surface defects, and tested to understand the oxide structural evolution when interacting with chloride ions in aqueous media. Chemical thinning of oxide film and pit nucleation is observed below the implemented surface defect. Also mechanical failure of bulk substrate is found, implying high stress build-up around pitting nucleation or highly corroded sites. As confirmed by morphology of the corroded passive film in the preliminary study, chloride ion adsorption and breakdown of surface oxide thin film do not yield significant lateral diffusion, yielding local build-up of Cu−Cl clusters. Dissolved copper atoms gain higher charge than copper oxides, and attract nearby chloride ions. As nearby chloride ions are consumed by the local corrosion, locally chloride deficient regions are produced. Because of increased Coulomb interactions by highly charged copper cations and low density of chloride ions, far-field chloride ions will diffuse or migrate into the locally corroded sites.

The failure of oxide thin film is driven mostly by chemical interactions but results in mechanical or structural instability as well.

AUTHOR INFORMATION

Corresponding Author

*E-mail: bjeon@seas.harvard.edu.

Notes

The authors declare no competing financial interest.

ACKNOWLEDGMENTS

This work has been supported by the Office of Naval Research with contract No. N00014-10-1-0346. The computational facilities have been provided by the Center for Nanoscale Materials (CNM) of Argonne National laboratory and Center for Nanoscale Systems (CNS) - National Nanotechnology Infrastructure Network (NNIN) at Harvard University. Use of the Center for Nanoscale Materials was supported by the U.S. Department of Energy, Office of Science, Office of Basic Energy Sciences, under Contract DE-AC02-06CH11357. We thank Dr. Bo-Kuai Lai for valuable discussion regarding the configuration of corrosion systems.

REFERENCES

(1) Paracchino, A.; Laporte, V.; Sivula, K.; Grätzel, M.; Thimsen, E. *Nat. Mater.* **2011**, *10*, 456−461.
(2) Barth, C.; Reichling, M. *Nature* **2001**, *414*, 54−57.
(3) Al-Abadleh, H. A.; Grassian, V. H. *Surf. Sci. Rep.* **2003**, *52*, 63−161.
(4) Shin, H.-J.; Jung, J.; Motobayashi, K.; Yanagisawa, S.; Morikawa, Y.; Kim, Y.; Kawai, M. *Nat. Mater.* **2010**, *9*, 442−447.
(5) Freund, H.-J.; Kuhlenbeck, H.; Staemmler, V. *Rep. Prog. Phys.* **1996**, *59*, 283.
(6) Maurice, V.; Despert, G.; Zanna, S.; Bacos, M.; Marcus, P. *Nat. Mater.* **2004**, *3*, 687−691.
(7) Chowdhuri, A.; Sharma, P.; Gupta, V.; Sreenivas, K.; Rao, K. V. *J. Appl. Phys.* **2002**, *92*, 2172−2180.
(8) Hsieh, C.-T.; Chen, J.-M.; Lin, H.-H.; Shih, H.-C. *Appl. Phys. Lett.* **2003**, *83*, 3383−3385.
(9) Wang, W.; Liu, Z.; Liu, Y.; Xu, C.; Zheng, C.; Wang, G. *Appl. Phys. A: Mater. Sci. Process.* **2003**, *76*, 417−420.
(10) Anandan, S.; Wen, X.; Yang, S. *Mater. Chem. Phys.* **2005**, *93*, 35−40.
(11) Bennici, S.; Gervasini, A. *Appl. Catal., B* **2006**, *62*, 336−344.
(12) Frankel, G. S. *J. Electrochem. Soc.* **1998**, *145*, 2186−2198.
(13) Frankel, G. S.; Sridhar, N. *Mater. Today* **2008**, *11*, 38−44.
(14) Khaled, K. *Mater. Chem. Phys.* **2008**, *112*, 104−111.
(15) Lee, H. P.; Nobe, K.; Pearlstein, A. J. *J. Electrochem. Soc.* **1985**, *132*, 1031−1037.
(16) Milošev, I.; Metikoš-Hukovic, M. *J. Electrochem. Soc.* **1991**, *138*, 61−67.
(17) Sathiyanarayanan, S.; Sahre, M.; Kautek, W. *Corros. Sci.* **1999**, *41*, 1899−1909.
(18) Chmielová, M.; Seidlerová, J.; Weiss, Z. *Corros. Sci.* **2003**, *45*, 883−889.
(19) Falkenberg, F.; Fushimi, K.; Seo, M. *Corros. Sci.* **2003**, *45*, 2657−2670.
(20) Yabuki, A.; Murakami, M. *Corrosion* **2007**, *63*, 249−257.
(21) Christy, A.; Lowe, A.; Otieno-Alego, V.; Stoll, M.; Webster, R. *J. Appl. Electrochem.* **2004**, *34*, 225−233.
(22) Schmitt, G.; Plagemann, P.; Slavcheva, E. *Mater. Corros.* **2001**, *52*, 439−444.
(23) Yeow, C. W.; Hibbert, D. B. *J. Electrochem. Soc.* **1983**, *130*, 786−790.
(24) Hack, H. P.; Pickering, H. W. *J. Electrochem. Soc.* **1991**, *138*, 690−695.
(25) Núñez, L.; Reguera, E.; Corvo, F.; González, E.; Vazquez, C. *Corros. Sci.* **2005**, *47*, 461−484.
(26) Otmačić, H.; Telegdi, J.; Papp, K.; Stupnišek-Lisac, E. *J. Appl. Electrochem.* **2004**, *34*, 545−550.
(27) Sherif, E. M.; Park, S.-M. *J. Electrochem. Soc.* **2005**, *152*, B205−B211.
(28) Hamelin, A. In *Modern Aspects of Electrochemistry*; Conway, B., White, R., Bockris, J., Eds.; Plenum Press, 1980; Vol. *16*, p 1.
(29) El Warraky, A.; El Shayeb, H.; Sherif, E. *Anti-corros. Meth. Mater.* **2004**, *51*, 52−61.
(30) Bacarella, A. L.; J. C. Griess, J. *J. Electrochem. Soc.* **1973**, *120*, 459−465.
(31) Lee, H. P.; Nobe, K. *J. Electrochem. Soc.* **1986**, *133*, 2035−2043.
(32) Suleiman, I. A.; Radny, M. W.; Gladys, M. J.; Smith, P. V.; Mackie, J. C.; Kennedy, E. M.; Dlugogorski, B. Z. *Phys. Chem. Chem. Phys.* **2011**, *13*, 10306−10311.
(33) Altarawneh, M.; Radny, M. W.; Smith, P. V.; Mackie, J. C.; Kennedy, E. M.; Dlugogorski, B. Z.; Soon, A.; Stampfl, C. *J. Chem. Phys.* **2009**, *130*, 184505.

(34) Suleiman, I. A.; Radny, M. W.; Gladys, M. J.; Smith, P. V.; Mackie, J. C.; Kennedy, E. M.; Dlugogorski, B. Z. *J. Phys. Chem. C* **2011**, *115*, 13412−13419.
(35) Stampfl, C.; Ganduglia-Pirovano, M. V.; Reuter, K.; Scheffler, M. *Surf. Sci.* **2002**, *500*, 368−394.
(36) Jeon, B.; Sankaranarayanan, S. K. R. S.; van Duin, A. C. T.; Ramanathan, S. *J. Chem. Phys.* **2011**, *134*, 234706.
(37) van Duin, A. C. T.; Dasgupta, S.; Lorant, F.; Goddard, W. A. *J. Phys. Chem. A* **2001**, *105*, 9396−9409.
(38) Marx, D.; Tuckerman, M. E.; Hutter, J.; Parrinello, M. *Nature* **1999**, *397*, 601−604.
(39) Marx, D. *ChemPhysChem* **2006**, *7*, 1848−1870.
(40) van Duin, A. C. T.; Bryantsev, V. S.; Diallo, M. S.; Goddard, W. A.; Rahaman, O.; Doren, D. J.; Raymand, D.; Hermansson, K. *J. Phys. Chem. A* **2010**, *114*, 9507−9514.
(41) Rahaman, O.; van Duin, A. C. T.; Bryantsev, V. S.; Mueller, J. E.; Solares, S. D.; Goddard, W. A.; Doren, D. J. *J. Phys. Chem. A* **2010**, *114*, 3556−3568.
(42) Abell, G. C. *Phys. Rev. B* **1985**, *31*, 6184−6196.
(43) Tersoff, J. *Phys. Rev. Lett.* **1988**, *61*, 2879−2882.
(44) Brenner, D. W. *Phys. Rev. B* **1990**, *42*, 9458−9471.
(45) Mortier, W. J.; Ghosh, S. K.; Shankar, S. *J. Am. Chem. Soc.* **1986**, *108*, 4315−4320.
(46) Janssens, G. O. A.; Baekelandt, B. G.; Toufar, H.; Mortier, W. J.; Schoonheydt, R. A. *J. Phys. Chem.* **1995**, *99*, 3251−3258.
(47) Chenoweth, K.; van Duin, A. C. T.; Goddard, W. A. *J. Phys. Chem. A* **2008**, *112*, 1040−1053 PMID: 18197648..
(48) http://www.jmol.org/, OpenMP The OpenMP API specification for parallel programming.
(49) Tarmyshov, K. B.; Müller-Plathe, F. *J. Chem. Inf. Model.* **2005**, *45*, 1943−1952.
(50) Berendsen, H.; Postma, J.; van Gunsteren, W.; Di Nola, A.; Haak, J. *J. Chem. Phys.* **1984**, *81*, 3684−3690.
(51) Baroux, B. In *Corrosion Mechanisms in Theory and Practice*; Marcus, P., Ed.; Marcel Dekker: New York, 2002; p 311.
(52) Haynes, W. M., Ed. *CRC Handbook of Chemistry and Physics*, 91st ed.; CRC PRESS, 2010.
(53) Jeon, B.; Sankaranarayanan, S. K.; Ramanathan, S. *J. Phys. Chem. C* **2011**, *115*, 6571−6580.
(54) Jeon, B.; Sankaranarayanan, S. K. R. S. Hybrid parallelization of a reactive molecular dynamics code for multiple-core processor clusters. 2012, in preparation.
(55) Schall, P.; Cohen, I.; Weitz, D.; Spaepen, F. *Science* **2004**, *305*, 1944−1948.
(56) Pidaparti, R. M.; Patel, R. K. *Corros. Sci.* **2010**, *52*, 3150−3153.
(57) Leiva-García, R.; García-Antón, J.; noz Portero, M. M. *Corros. Sci.* **2010**, *52*, 2133−2142.